

# Exploring percolation phase transition in the three-dimensional Ising model with machine learning

Ranran Guo,<sup>1</sup> Xiaobing Li,<sup>1</sup> Shiyang Chen,<sup>2</sup> and Zhiming Li<sup>1,\*</sup>

<sup>1</sup>*Key Laboratory of Quark and Lepton Physics (MOE) and Institute of Particle Physics, Central China Normal University, Wuhan 430079, China*

<sup>2</sup>*Department of Physics, Swansea University, SA2 8PP, Swansea, United Kingdom*

The percolation phase transition plays a significant role in understanding the Quantum Chromodynamics (QCD) phase diagram, particularly in the study of the Quark-gluon Plasma and the critical point in high energy nuclear physics. It is expected that the QCD critical point belongs to the three-dimensional (3D) Ising universality class. In this study, we explore the percolation phase transition within the 3D cubic Ising model by employing two machine learning algorithms: Principal Component Analysis and the Domain Adversarial Neural Network. Our findings reveal the effectiveness of machine learning techniques in distinguishing different phases during the percolation transition. Through the finite-size scaling analysis on the output of the neural networks, the critical temperature and a correlation length exponent in the geometrical percolation transition are extracted and compared to those in the thermal magnetization phase transition within the 3D Ising model. These results offer valuable insights to our understanding of QCD phase transitions in relativistic heavy-ion collisions.

## I. INTRODUCTION

The primary objective of relativistic heavy-ion collision is to investigate the phase diagram of Quantum Chromodynamics (QCD) and to search for the critical point (CP) of phase transition from hadron to Quark-gluon Plasma (QGP) [1–4]. At the region of a vanishing or small baryon chemical potential  $\mu_B$ , the prevailing understanding is that the transition occurs as a smooth crossover [5]. According to predictions from effective field theory, at low temperature  $T$  and high  $\mu_B$ , the phase transition is anticipated to be of the first-order nature [6, 7]. The CP denotes the terminus of the first-order phase transition line. Currently, physicists are focused on exploring both the boundary of the QCD phase diagram and the position of the CP as these subjects are of considerable interests [8, 9].

The QCD phase diagram is not yet well understood, either experimentally or theoretically. The constraints of lattice QCD calculations are such that they are currently confined to scenarios with vanishing or small values of  $\mu_B$  due to the sign problem [10, 11], which drastically complicates computations involving non-zero chemical potentials. Consequently, various phenomenological models, including spin models, have been put forth to explore phase transitions due to the universal aspects of critical phenomena [12–16]. A phase transition occurs due to spontaneous symmetry breaking. Systems with the same symmetry belong to the same universality class, displaying identical critical exponents and potentially analogous critical behavior. The conjecture is that the CP of QCD belongs to the  $Z(2)$  universality class, which is the same as the 3D Ising model [1, 17–20]. Drawing on the map-

ping of a parametric equation of state within the 3D Ising model, it becomes possible to construct a relation between the Ising phase diagram in the  $(T, H)$  plane and that of QCD in the  $(T, \mu_B)$  plane [21, 22].

Percolation theory serves as a statistical mechanism dedicated to investigate the behavior of interconnected clusters within various media. It studies the connectivity of objects within a network structure and how this connectivity affects the macro-scale properties of the system. In the percolation theory, clusters hold significant importance [23]. The emergence of percolation clusters, in which the microscopic elements become connected and form a sample-spanning path across the system, is suggested to be an indicator of the occurrence of a continuous percolation phase transition [24]. This theory has demonstrated its utility in exploring the distinctive features of the QCD phase transition. It has been used to predict the critical density required for the formation of QGP [25, 26], as well as to dissect the initial phase of deconfinement transition in heavy-ion collisions [27–29]. Additionally, the QGP to hadron cross-over transition has been characterized via the temperature dependence of the shear viscosity over entropy density ratio, utilizing the percolation framework within the Color String Percolation Model [30].

In statistical physics, the concept of the order parameter finds extensive application in categorizing distinct states of matter and detecting phase transitions within a given system. However, the intricate nature of robust interactions introduces considerable challenges in ascertaining the order parameter associated with the QCD phase transition and subsequently measuring it through experiments. Recent advancements have proposed the integration of machine learning (ML)[31, 32] as a promising approach to delve into this intricate physical quandary[33, 34]. Empirical evidence now substantiates that ML techniques hold the capability to effectively discern the order parameter [35–40], distinguish phases and

---

\*Electronic address: lizm@mail.ccnu.edu.cn

identify thermal magnetization phase transitions [41–45] within the Ising model by various ML methodologies.

The investigations on the Ising model in the market have commonly employed magnetization as an order parameter to explore the thermal magnetization phase transition under alterations in temperature or external field. This thermal magnetization transition is characterized by a pivotal Curie temperature ( $T_c$ ). When surpassing  $T_c$ , the system assumes a disordered phase, but when dropping below it, the system transitions into an ordered phase characterized by a non-zero spontaneous magnetization. The geometrical percolation transition, on the other hand, is related to the connectivity of spin clusters. Envision a lattice of spins where each spin interacts with its nearest neighbors. At a specific critical percolation threshold, denoted as a certain temperature  $T_p$ , the system experiences a percolation transition. When across  $T_p$ , the spin clusters start to merge and form a large cluster that spans the entire lattice in the data sample. Recent studies have brought to light that within the ordered phase of the 3D Ising model, a percolation transition materializes in the domain boundaries of spin clusters when roughly 13% of spins represent the minority [46]. Through an exploration of the fractal arrangement and scaling properties of a two-dimensional slice from the 3D Ising model, it has been found that the percolation transition coincides with the Curie point, exclusively considering geometric spin (GS) clusters [47]. However, the precise solution of the critical temperature and the theoretical values associated with critical exponents in the context of geometrical percolation phase transition within the 3D Ising model still remain unsolved.

In this work, we confront these challenges by using the power of unsupervised and semi-supervised ML methods. These approaches do not require prior knowledge of order parameters or any additional information. We demonstrate the efficacy of both ML techniques in categorizing different phases of the percolation transition. Furthermore, we try to extract the critical temperature and a critical exponent associated with the percolation phase transition within the Ising model directly from the output layer of the neural networks. The subsequent sections of this paper are structured as follows: In Section II, we offer a brief introduction to the percolation transition in the 3D Ising model. Section III gives an overview of the network algorithms employed in this study. Moving on to Section IV and V, we present and discuss the results pertaining to the identification of percolation phase transitions within the Ising model, utilizing the Principal Component Analysis and the Domain Adversarial Neural Network methods, respectively. Finally, in Section VI, we summarize our discoveries and provide an outlook for future directions.

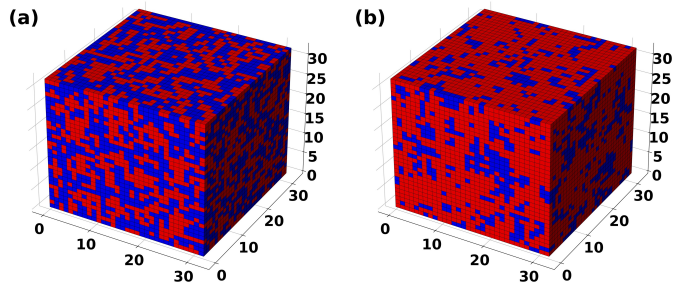


FIG. 1: (color online) The spin configurations of the 3D Ising model with a lattice size of  $L = 32$  are depicted as (a) in the absence of percolation clusters at  $T = 7.52$ , and (b) in the presence of a percolation cluster at  $T = 4.42$ .

## II. PERCOLATION TRANSITION IN THE 3D ISING MODEL

Ising model [48] is a classic spin model utilized for investigating phase transitions. We consider a three-dimensional cubic lattice composed of  $N = L \times L \times L$  sites with periodic boundary conditions. Each site is occupied by a spin,  $s_i$ . We assume that the spin of individual site can have one of the two states, either spin-up,  $s_i = +1$ , or spin-down,  $s_i = -1$ . In this analysis, we only study the 3D Ising model in zero external field, as described by the Hamiltonian

$$\mathcal{H} = -J \sum_{\langle ij \rangle} s_i s_j, \quad (1)$$

where  $J$  is known as the coupling constant between two spins  $s_i$  and  $s_j$ . Here we set  $J = 1$  as the energy unit.

The Wolff algorithm, a Monte-Carlo method, is frequently employed to generate equilibrium configurations of the Ising model under varying conditions, such as changes in system size or temperature. In the present investigation, we explore a temperature range spanning from  $T = 0.02$  to  $T = 7.92$  with external magnetic field  $H = 0$ . We generate a set of 2000 independent spin configurations for each selected temperature with a given system size.

In the Ising model, clusters are identified as groups of neighboring sites with the same spin direction. As the temperature of the system changes, the spins tend to align with their neighbors due to interactions between them. The percolation phase transition refers to a significant change in the way clusters of aligned spins form and extend within the whole lattice at a certain critical temperature  $T_p$ . Away from this critical temperature, small clusters of aligned spins are isolated and do not span the entire lattice. However, as the temperature crosses  $T_p$ , these smaller clusters start to coalesce and connect, leading to the emergence of a percolating cluster that spans the lattice from one edge to another. This percolating cluster signifies a sudden change in the system behavior, as the alignment of spins becomes correlated over long distances.

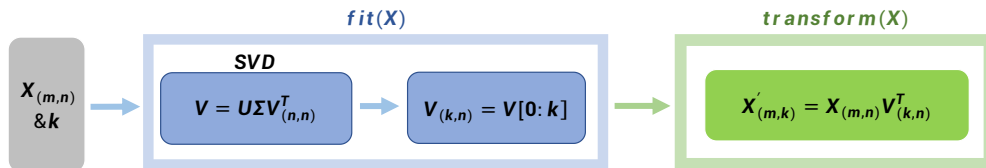


FIG. 2: (color online) The PCA architecture used in our analysis.

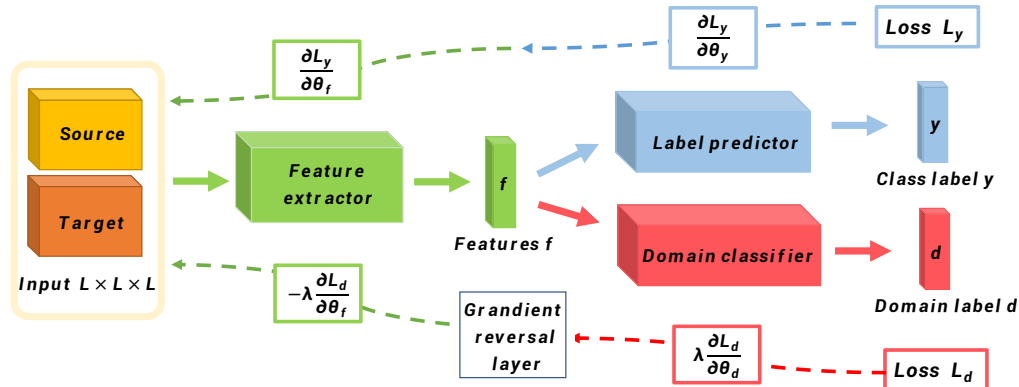


FIG. 3: (color online) The DANN architecture used in the analysis.

To facilitate an intuitive comprehension, Fig. 1 (a) shows the spin configurations within the 3D Ising model for a system size of  $32 \times 32 \times 32$  at a temperature of  $T = 7.52$ . In this depiction, red lattices represent spin-up orientations, while blue ones denote spin-down. At high temperature, owing to the stochastic distribution of the spin states, no percolation clusters are discernible. Moving to Fig. 1 (b), which illustrates the configuration at a low temperature of  $T = 4.42$ , we observe a predominant cluster colored in red. This cluster spans the lattice between opposing edges, signifying the presence of percolation clusters. The percolation transition is of great interest because it often leads to emergent behaviors and critical phenomena, where small changes in a model parameter can lead to drastic alterations in the overall behavior of the system.

### III. MACHINE LEARNING METHODOLOGY

Supervised learning, unsupervised learning, and semi-supervised learning are fundamental paradigms in machine learning [49], each with different approaches and applications. Supervised learning involves training a model on labeled data, where input-output pairs are provided, enabling the model to learn patterns and make accurate predictions on new, unseen data. Unsupervised learning, on the other hand, deals with unlabeled data, aiming to uncover inherent structures, clusters, or relationships within the data. Semi-supervised learning merges elements of both, incorporating labeled and un-

labeled data to enhance model performance. By leveraging the small amount of labeled data alongside the larger pool of unlabeled data, semi-supervised learning strikes a balance between efficiency and accuracy, making it valuable when acquiring fully labeled datasets is expensive or time-consuming.

To enhance the versatility and future applicability of our approach, we use both the unsupervised Principal Component Analysis (PCA) method and the semi-supervised Domain Adversarial Neural Network (DANN) methodology in this study. It allows to extend the possible utility of our methods to the analysis of experimental data, ensuring a broader scope and improved adaptability for future applications in high energy physics.

PCA is among the most widely utilized multivariate techniques [50], with its origins tracing back to Pearson's pioneering work in statistics [51]. Pearson's formulation involves identifying optimal lines and planes to closely align with point distributions in space. PCA aims to simplify complex datasets by identifying a new set of orthogonal axes, called principal components, that capture the most significant variations in the data. These components are ordered in terms of the amount of variance they explain, allowing for the reduction of high-dimensional data into a lower-dimensional space while retaining as much relevant information as possible. Functioning as a classic example of unsupervised learning, PCA finds extensive application in tasks such as data clustering and dimensionality reduction [52–54].

The sketch in Fig. 2 illustrates the network architecture employed by the PCA algorithm in this investiga-

tion. It can be segmented into two main components: the fit stage and the transform stage. To begin with, the network takes as input the preprocessed data from the largest clusters denoted as  $X_{(m,n)}$ , along with the predetermined number of principal component features, denoted as  $k$ . In the fit stage, PCA computes the mean and covariance matrix for the dataset  $X_{(m,n)}$ . Subsequently, the Singular Value Decomposition (SVD) decomposes the covariance matrix into eigenvalues and their corresponding eigenvectors, which are denoted as  $V$ . Given the predefined value of  $k$ , the network proceeds to identify the principal components of the data, resulting in  $V_{(k,n)}$ . Shifting to the transform stage, the network executes a projection of the original data  $X$  onto the selected principal components  $V_{(k,n)}$ . As a result, the data is transformed into a reduced-dimensional representation, denoted as  $X'_{m,k}$ . This accomplishment effectively realizes the objectives of both dimensionality reduction and feature extraction.

DANN [55] is a specific type of transfer learning [56, 57] that emphasizes the mapping relationship between labeled source domain data and unlabeled target domain data, rather than the clustering and dimensionality reduction features provided by PCA. DANN uniquely integrates deep feature learning and domain adaptation, enabling the classification decision to be based on both discriminative and domain-invariant features for accurate data classification. By leveraging DANN, the classification process can effectively utilize features that are both informative and immune to domain variations.

The overall structure of DANN is shown in Fig. 3, comprising three main components: a feature extractor (green), a label predictor (blue), and a domain classifier (red). The feature extractor captures informative features from the input data, transforming them into the feature vector  $f$ . The label predictor is responsible for training the network to classify the input data based on the feature vector  $f$ . The domain classifier, on the other hand, predicts the domain labels of feature vectors from both the source and target domains, enabling the analysis of data origin. In our neural network architecture, the feature extractor and label predictor form a conventional feedforward neural network. Additionally, the feature extractor constitutes an adversarial network by connecting a gradient reversal layer to the domain classifier. The loss function for the domain adversarial network comprises two components: one for the label predictor and another for the domain classifier. The primary objective of network training is to minimize both components of the loss function. This allows the label predictor to accurately classify input data while making it challenging for the domain classifier to differentiate the domain to which the data belongs.

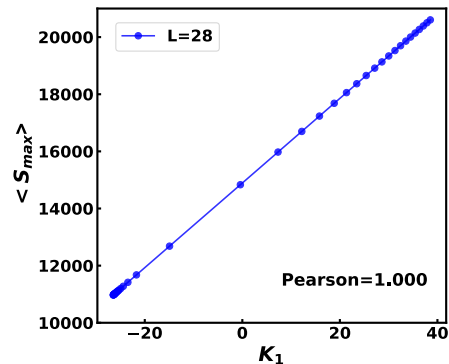


FIG. 4: (color online) The average size of the largest clusters as a function of the output of the first principal component in PCA with  $L = 28$ .

#### IV. ML THE PERCOLATION TRANSITIONS IN THE ISING MODEL BY PCA

The geometrical percolation transition typically involves several key quantities, such as percolation strength, the largest cluster size, average cluster size, as discussed in reference [58]. The cluster size, denoted as  $S$ , is determined by the count of spin sites it encompasses. To ensure sufficient data for subsequent calculations, our primary focus is on the largest cluster size, referred to as  $S_{max}$ , which is influenced by both temperature and volume of the system.

It has been verified that  $S_{max}$  plays a crucial role in understanding the behavior of systems undergoing a phase transition from a disconnected state to a connected state [14]. The appearance of a percolating cluster serves as a critical indicator of a phase transition within the system. Along with other extensive variables such as susceptibility and correlation length, the size of the largest cluster obeys scaling laws near the critical point. Studying how the size of the largest cluster scales with the distance from the critical point provides valuable information on the universality class of the phase transition. Understanding the size and structure of the largest cluster is essential for gaining insights into the critical behavior of percolating systems and characterizing overall connectivity properties.

In the thermal magnetization phase transition of the Ising model, it has been found that the first principal component possess the greatest explained variance [38]. The results derived from the first principal component confirm its linear relationship with magnetization. This implies that the first PCA of the input data can effectively capture and learn about magnetization, which is the characteristic order parameter for the thermal magnetization transition in the 3D Ising model. To assess the capacity of the unsupervised ML method for learning and identifying important features associated with the largest cluster size from the input data in the percolation transition, we choose PCA methodology with one principal

component.

We generate event samples for a given system size of  $L = 28$  and cover a temperature range spanning from  $T = 3.52$  to  $T = 5.52$ . The raw spin configurations of the largest cluster in each sample of the 3D Ising model are used as input data for the PCA network architecture, as depicted in Fig. 2. Subsequently, we compute the average sizes of the 2000 largest clusters at each temperature point and conduct a Pearson correlation analysis with respect to the first principal component obtained from PCA. The correlation between the average size of the largest clusters  $\langle S_{max} \rangle$  and the first principal component  $K_1$  of the PCA is graphically illustrated in Fig. 4. Our findings reveal a linear relationship between  $\langle S_{max} \rangle$  and  $K_1$ . The computed Pearson correlation coefficient of 1.00 suggests a strong positive correlation between  $\langle S_{max} \rangle$  and  $K_1$ .

As we know, the first principal component  $K_1$  represents the newly defined coordinate axis within PCA. This axis encapsulates the highest amount of information and exhibits the greatest power in distinguishing patterns in the data. It plays the most significant role in accounting for variations in the data and excels at elucidating data changes. The observed strong positive correlation between the average size of the largest clusters  $S_{max}$  and  $K_1$  provides further confirmation that the largest cluster carries a substantial amount of critical system information, and this information can be effectively acquired from the first principal component of PCA in the geometric percolation phase transition.

We will now explore the capability of PCA in identifying different phases and investigating the critical temperature associated with the percolation transition within the 3D Ising model. As detailed in Sec. II, the Ising model undergoes a geometric percolation phase transition at a critical temperature  $T_p$ . This transition separates a disconnected state at high temperatures from a fully connected state at low temperatures. To achieve this, we establish a PCA network to conduct unsupervised learning directly on samples of spin configurations.

The numerical results obtained from five different system sizes and spanning the temperature range  $T \in [3.52, 5.52]$  are illustrated in Fig. 5 (a). The first principal component  $K_1$  initially exhibits a gradual decrease as the temperature increases for all sizes considered. This is followed by a sharp drop as the temperature approaches a specific point, ultimately reaching equilibrium at higher temperatures. Notably, the  $K_1$  values for different sizes intersect at a particular temperature, precisely corresponding to the critical temperature of the percolation phase transition. This demonstrates the effectiveness of PCA as a methodology for classifying the two different phases of the percolation transition in the 3D Ising model.

We conduct five independent iterations of the PCA network, each with different finite size  $L$ . Subsequently, we employ a finite-size scaling analysis to estimate the percolation transition temperature in the infinite  $L$  limit,

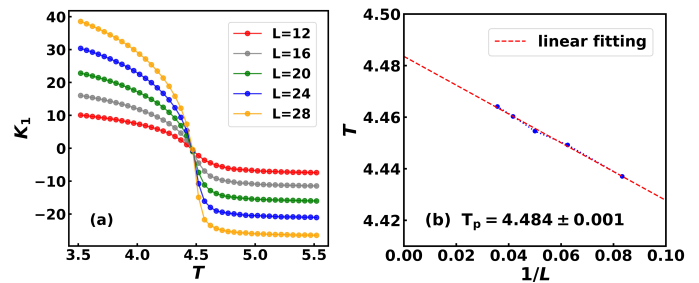


FIG. 5: (color online)(a) The first principal component of PCA as a function of temperature for five different system sizes. (b) Finite-size scaling analysis to determine percolation critical temperature based on the first principal component.

using information derived from the first principal component [38, 59]. The critical temperature  $T_p$  is achieved by extrapolating through a linear fit as the limit  $1/L$  approached zero, as illustrated in Fig. 5 (b). The statistical errors are estimated using the standard deviation and are found to be smaller than the size of the data points. The critical temperature determined from the fitting process yields  $T_p = 4.484 \pm 0.001$ . We would point out that this critical temperature for the percolation transition in the 3D Ising model is slightly lower than the critical temperature for the thermal magnetization phase transition, which is  $T_c = 4.512 \pm 0.001$  as reported in references [59–61]. This finding is qualitatively consistent with the results in reference [62, 63].

## V. ML THE PERCOLATION TRANSITIONS BY DANN

Domain Adversarial Neural Network is a deep learning technique mainly applied in the domain adaptation field. The primary advantage of DANN is its ability to adapt a machine learning model from one domain to another, particularly when the source and target domains have different data distributions. The network structure of DANN used in this analysis is illustrated in Fig. 3. This neural network is trained in such a way that the feature representations of the two domains become indistinguishable to the domain classifier.

In our analysis, we characterize percolation clusters at extremely low temperatures and with no percolation phenomenon at exceedingly high temperatures in the Ising model. Consequently, we designate the data at low and high temperatures as the source domain data during DANN network training, with the unlabeled one in the intermediate temperature range regarded as the target domain data. To establish the optimal temperature range for each scale, we employ a technique involving the fixation of either low-temperature or high-temperature labels while decreasing the high-temperature labels or increasing the low-temperature labels, respectively. The specific selection of the temperature range for target domain

System size $L$	12	16	20	24	28
The optimal temperature range of the target domain	[3.92, 4.52]	[4.27, 4.52]	[4.27, 4.57]	[4.37, 4.57]	[4.42, 4.52]

TABLE I: Selection of optimal temperature range of target domain in DANN.

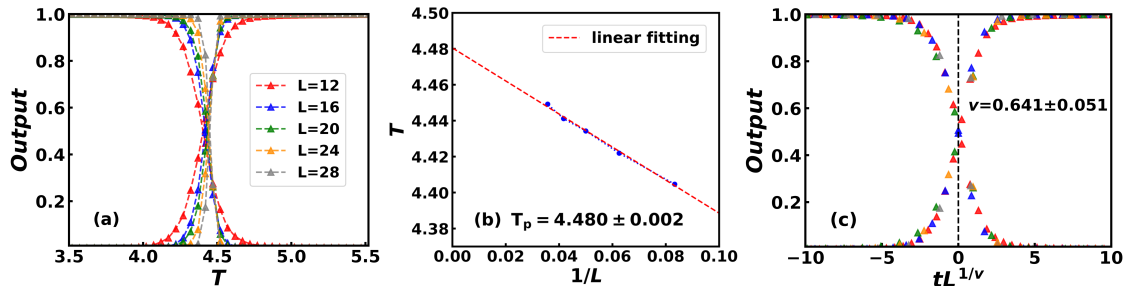


FIG. 6: (color online) (a) The output layer averaged over test sets of DANN as a function of temperature for five different system sizes. (b) Finite-size scaling analysis to determine percolation critical temperature. (c) Data collapse of the average output layer as a function of  $tL^{1/\nu}$ , where  $t = (T - T_p)/T_p$  is the reduced temperature.

data at various system sizes is outlined in Table I. The source domain data can then be annotated with suitable labels according to the target domain range. In this process, DANN learns the mapping relationship between the source domain data and the target domain data. The ultimate label predictor proves effective at accurately forecasting the percolation classification of unlabeled data in the target domain through the utilization of domain adaptation and back-propagation techniques.

After training the DANN on the optimal domain, we assess samples at various temperatures, allowing the DANN to classify them to either phase '1' or phase '0', indicating the presence or absence of the percolation transition, respectively. On the output side, DANN returns the probability for each configuration belonging to phase '1' or '0'. The numerical results obtained at various system sizes at a vanishing magnetic field are illustrated in Fig. 6 (a). The average outputs of different sizes cross at a specific temperature corresponding to the critical temperature. It infers that the DANN can successfully classify the two different phases in the percolation transition in the Ising model.

To determine the percolation critical temperature, we conduct DANN training at five different sizes and extrapolate the results to  $L \rightarrow \infty$ , following the same procedure outlined in Sec. IV for the PCA network. The outcomes are presented in Fig. 6 (b). The obtained critical temperature for the percolation transition,  $T_p = 4.480 \pm 0.002$ , is in agreement with the result from the PCA network. This temperature is slightly lower than the critical temperature associated with the thermal magnetization phase transition in the 3D Ising model.

The critical exponents associated with the 3D Ising model play a crucial role in characterizing the behavior

of various thermodynamic and correlation functions as the system approaches the critical point. They are considered universal in nature, *i.e.*, they remain unchanged regardless of the specific characteristics of the physical system. Among these exponents, the correlation length exponent  $\nu$  holds significance as it reveals how the correlation length undergoes a pronounced divergence near the critical point. This divergence is described by the relationship between the correlation length  $\xi$  and temperature, expressed as  $\xi \sim |T - T_p|^{-\nu}$ . In the case of a finite system, it is expected that the correlation length scales proportionally to the size of the system. Consequently, one can establish a connection between the temperature and the system size, characterized by the expression  $|T - T_p| \sim L^{-1/\nu}$ .

To extract the critical exponent  $\nu$ , we employ a finite-size scaling analysis and the results are shown in Fig. 6 (c). What becomes evident from the figure is that as different system sizes are considered, they exhibit a compelling convergence with  $T_p = 4.480 \pm 0.002$  and  $\nu = 0.641 \pm 0.051$ . This value of the correlation length exponent for the percolation phase transition slightly exceeds the one for the thermal magnetization phase transition, which is reported as  $\nu = 0.63 \pm 0.01$  obtained using the MC method [60, 61] and renormalization group theory [59].

## VI. CONCLUSIONS AND OUTLOOK

In summary, we employ both unsupervised and semi-supervised machine learning techniques to investigate percolation phase transitions within the 3D Ising model. We find a linear correlation between the average size of

the largest clusters and the primary component of PCA, suggesting that the largest clusters contain sufficient information pertaining to the percolation transition. We use two distinct machine learning approaches by utilizing the spin configurations from the largest clusters as input data, and apply the finite-size scaling method to estimate the critical temperature of the percolation phase transition. Both of these machine learning methodologies effectively classify disconnected states at higher temperatures and fully connected states at lower temperatures. As a result, we determine the critical temperature for the percolation transition to be  $T_p = 4.484 \pm 0.001$  and  $T_p = 4.480 \pm 0.002$  by using PCA and DANN, respectively. These temperatures are found to be a little bit lower than the critical temperature for the thermal magnetization phase transition. The extracted correlation length exponent is found to be  $\nu = 0.641 \pm 0.051$ , which is slightly greater than the critical exponent associated with the thermal magnetization phase transition in the 3D Ising model.

In heavy-ion collisions, the percolation transition holds significant importance within the context of QCD phase transitions. It provides a theoretical framework for understanding the critical behavior, cluster formation, and experimental signatures associated with the transition from hadronic matter to the Quark-gluon Plasma. The

machine learning methods developed in this study possess the remarkable ability to require minimal or even no training data to identify phase transitions, extract critical temperature and critical exponents. This capability allows for the convenient application in the investigation of criticality in high energy experimental data or other Monte-Carlo models, which could help to explore the underlying physical mechanisms governing the QCD phase transition.

### Acknowledgments

We are grateful to Prof. Yuanfang Wu, Mingmei Xu, Lizhu Chen and Dr. Feiyi Liu for fruitful discussions and comments. We further thank Prof. Hengtong Ding for providing us with computing resources. The numerical simulations have been performed on the GPU cluster in the Nuclear Science Computing Center at Central China Normal University (NSC<sup>3</sup>). This work is supported by the National Key Research and Development Program of China (No. 2022YFA1604900) and the National Natural Science Foundation of China (No. 12275102).

R.G. and X.L. contributed equally to this work.

- 
- [1] M. Stephanov, K. Rajagopal, and E. Shuryak, Phys. Rev. Lett. 81, 4816 (1998).
  - [2] J. Adams et al.(STAR Collaboration), Nucl. Phys. A 757, 102 (2005).
  - [3] M. Asakawa, U. W. Heinz, and B. Muller, Phys. Rev. Lett. 85, 2072 (2000).
  - [4] V. Koch, A. Majumder, and J. Randrup, Phys. Rev. Lett. 95, 182301 (2005).
  - [5] Y. Aoki, G. Endrodi and Z. Fodor, et al, Physics Letters B 643, 46 (2006).
  - [6] M. Asakawa and K. Yazaki, Nucl. Phys. A 504, 668 (1989).
  - [7] E. S. Bowman and J. I. Kapusta, Phys. Rev. C 79, 015202 (2009).
  - [8] Z. Fodor and S. D. Katz, JHEP 2004, 50 (2004).
  - [9] R. V. Gavai and S. Gupta, Phys. Rev. D 78, 114503 (2008).
  - [10] J. N. Guenther, Eur. Phys. J. A 57, 136 (2021).
  - [11] A. Bazavov et al. (HotQCD Collab.), Phys. Rev. D 96, 074501 (2017).
  - [12] X. Li, R. Guo, Y. Zhou et al., Chin. Phys. C 47, 034101 (2023).
  - [13] X. Li, M. Xu, Y. Zhang et al., Phys. Rev. C 105, 064904 (2022).
  - [14] L. Chen, Y. Y. Zhao, X. Li et al., Int. J Mod. Phys. E 30, 2150056 (2021).
  - [15] X. Pan, L. Chen, X. S. Chen et al., Nucl. Phys. A 913, 206 (2013).
  - [16] X. Li, Y. Zhong, R. Guo et al., arXiv: 2305.18468 (2023).
  - [17] R. D. Pisarski and F. Wilczek, Phys. Rev. D 29, 338 (1984).
  - [18] M. Asakawa, J. Phys. G: Nucl. Part. Phys. 36, 064042 (2009).
  - [19] P. de Forcrand and O. Philipsen, Phys. Rev. Lett. 105, 152001 (2010).
  - [20] F. Karsch, E. Laermann, and C. Schmidt, Phys. Lett. B 520, 41 (2001).
  - [21] M. A. Stephanov, Phys. Rev. Lett. 107, 052301 (2011).
  - [22] P. Parotto, PoS. CPOD2017, 036 (2017).
  - [23] A. Coniglio, Phys. Rev. B 13, 2194 (1976).
  - [24] M. Xu, M. Yu and L. Liu, Phys. Rev. Lett. 100, 092301 (2008).
  - [25] G. Baym, Physica. A 96, 131 (1979).
  - [26] T. Celik, F. Karsch and H. Satz, Phys. Lett. B 97, 128 (1980).
  - [27] B. K. Srivastava, Nucl. Phys. A 926, 142 (2014).
  - [28] R. P. Scharenberg, B. K. Srivastava and C. Pajares, Phys. Rev. D 100, 114040 (2019).
  - [29] K. Goswami, D. Sahu and R. Sahoo , Phys. Rev. D 107, 014003 (2023).
  - [30] M. A. Braun, J. Dias de Deus, A. S. Hirsh et al., Phys. Rep. 599, 1 (2015).
  - [31] G. E. Hinton and R. R. Salakhutdinov, Science 313, 504 (2006).
  - [32] Y. L. Cun, Y. Bengio, and G. Hinton, Nature 521, 436 (2015).
  - [33] P. Mehta, M. Bukov, C. H. Wang et al., Phys. Rep. 810, 1 (2019).
  - [34] G. Carleo, I. Cirac, K. Cranmer et al., Rev. Mod. Phys. 91, 045002 (2019).
  - [35] L. Wang, Phys. Rev. B 94, 195105 (2016).
  - [36] S. J. Wetzel, Phys. Rev. E 96, 022140 (2017).

- [37] W. Hu, R. R. P. Singh and R. T. Scalettar, *Phys. Rev. E* 95, 062122 (2017).
- [38] R. Zhang, B. Wei, D. Zhang et al., *Phy. Rev. B* 99, 094427 (2019).
- [39] K. Kashiwa, Y. Kikuchi and A. Tanaka, *Prog. Theor. Exp. Phys.* 2019, 083A04 (2019).
- [40] D. W. Tola and M. Bekele, *Condens. Matter.* 8, 83 (2023).
- [41] J. Carrasquilla and R. G. Melko, *Nat. Phys.* 13, 431 (2017).
- [42] E. P. L. van Nieuwenburg, Y. H. Liu and S. D. Huber, *Nat. Phys.* 13, 435 (2017).
- [43] P. Ponte and R. G. Melko, *Phys. Rev. B* 96, 205146 (2017).
- [44] A. Canabarro, F. F. Fanchini, A. L. Malvezzi et al., *Phys. Rev. B* 100, 045129 (2019).
- [45] S. S. Funai, D. Giataganas, *Phys. Rev. Research.* 2, 033415 (2020).
- [46] M. Grady, *J. Phys.: Condens. Matter* 35, 285401 (2023).
- [47] A. A. Saberi and H. Dashti-Naserabadi, *EPL* 92, 67005 (2010).
- [48] V. E. Ising, *Z. Physik* 31, 253 (1925).
- [49] M. W. Berry, A. Mohamed, B. W. Yap, *Supervised and unsupervised learning for data science.* Springer Nature, 2019.
- [50] H. Abdi and L. J. Williams, *WIREs. Comp. Stat.* 2, 433 (2010).
- [51] F. R. S. Karl Pearson, *Philosophical Magazine.* 2, 559 (1901).
- [52] L. Wang, *Phys. Rev. B* 94, 195105 (2016).
- [53] S. J. Wetzel, *Phys. Rev. E* 96, 022140 (2017).
- [54] W. Yu and P. Lyu, *Physica A* 559, 125065 (2020).
- [55] Y. Ganin, E. Ustinova, H. Ajakan et al., *Journal of Machine Learning Research.* 17, 2096 (2016).
- [56] S. J. Pan and Q. Yang, *IEEE Trans. Knowl. Data. Eng.* 22, 1345 (2010).
- [57] C. Tan, F. Sun, T. Kong et al., *A survey on deep transfer learning.* Springer International Publishing, 2018.
- [58] A. A. Saberi, *Phys. Rep.* 578, 1 (2015).
- [59] A. Pelissetto and E. Vicari, *Phys. Rep.* 368, 549 (2002).
- [60] A. L. Talapov and H. W. J. Blote, *J. Phys. A: Math. Gen.* 29, 5727 (1996).
- [61] K. Binder, *E. Luijten, Phys. Rep.* 344, 179 (2001).
- [62] A. Coniglio, C. R. Nappi, F. Peruggi et al., *J. Phys. A: Math. Gen.* 10, 205 (1977).
- [63] H. Müller-Krumbhaar, *Phys. Lett. A* 48, 459 (1974).